Low-Photon-Number Optical Switching with a Single Quantum Dot Coupled to a Photonic Crystal Cavity

Ranojoy Bose,[1] Deepak Sridharan,[1] Hyochul Kim,[1] Glenn S. Solomon,[2] and Edo Waks[1,2,*]

[1]*Department of Electrical and Computer Engineering, IREAP, University of Maryland, College Park, Maryland 20742, USA*

[2]*Joint Quantum Institute, National Institute of Standards and Technology, and University of Maryland, Gaithersburg, Maryland 20899, USA*

(Received 3 August 2011; published 30 May 2012)

We demonstrate fast nonlinear optical switching between two laser pulses with as few as 140 photons of pulse energy by utilizing strong coupling between a single quantum dot (QD) and a photonic crystal cavity. The cavity-QD coupling is modified by a detuned pump pulse, resulting in a modulation of the scattered and transmitted amplitude of a time synchronized probe pulse that is resonant with the QD. The temporal switching response is measured to be as fast as 120 ps, demonstrating the ability to perform optical switching on picosecond timescales.

DOI: 10.1103/PhysRevLett.108.227402 PACS numbers: 78.67.Hc, 42.50.Ct, 42.65.Pc, 42.70.Qs

Nonlinear optical interactions are essential for a broad range of photonics applications. Such interactions enable all-optical switching, which plays a key role in increasing information bandwidth in telecommunications systems and could potentially reduce power consumption in computer processors [1]. Currently, there is also great interest in achieving optical switching at low photon numbers for applications in quantum information processing and quantum networking [2–4]. However, the majority of nonlinear optical processes rely on weak nonlinearities from a large ensemble of atomic systems and thus require high optical energies [5].

One promising method for reducing optical switching energies is to exploit the strong atom-light interactions between a quantum dot (QD) and a photonic crystal cavity. These interactions can enable the strong coupling regime where the cavity and QD mix to form new dressed polariton states, resulting in a modification of both the QD emission spectrum [6] and cavity spectrum [7–11]. In the strong coupling regime, the cavity-QD system can exhibit a large nonlinear optical response at low optical powers [12–16]. Controlling these nonlinearities on fast time scales could enable all-optical switching at extremely low energies.

Here we demonstrate that interaction between a single QD and a cavity in the strong coupling regime can be optically modulated on picosecond time scales to enable all-optical switching at extremely low energies. We study the specific example of a photonic crystal defect cavity coupled to an indium arsenide (InAs) QD. The response of the strongly coupled system is modulated by a picosecond pump laser pulse that induces a large nonlinear response, resulting in an observed modification of the transmission and scattering amplitude of a second incident probe pulse. The pump energy required to perform optical switching is measured to be as low as 140 photons. Switching response times as short as 120 ps are also reported, which are ultimately limited by bandwidth constraints imposed on the pump and probe pulses by the cavity-QD coupling strength. We implement this approach in a planar photonic crystal cavity-waveguide structure that is compatible with large scale integration for the development of complex devices on-a-chip.

Figure 1(a) shows a scanning electron micrograph of the device, and illustrates the switching concept. The device is composed of a gallium arsenide (GaAs) photonic crystal cavity evanescently coupled to a row defect waveguide. The initial wafer for device fabrication consisted of a 160 nm GaAs membrane with an InAs QD layer grown at the center (with QD density of approximately 10 μm^{-2}), on a 1 μm thick sacrificial layer of aluminum gallium arsenide ($Al_{0.78}Ga_{0.22}As$). Photonic crystal structures were defined using electron-beam lithography, followed by inductively coupled plasma dry etching and selective wet etching of the sacrificial AlGaAs layer. Details of the device design have been previously reported [11].

The pump and probe pulse are injected via grating couplers [17] into the waveguide. The probe pulse is collected either directly from the cavity (direct cavity scatter) or from the output coupler (transmitted waveguide signal) by spatial filtering. Figure 1(b) shows the cavity photoluminescence (PL) spectrum, attained by exciting the cavity with a 780 nm pump laser. The PL exhibits an emission peak for the cavity mode, along with additional emission peaks for several coupled QDs. The QD used for all measurements reported in this Letter is labeled in the figure. By fitting the cavity mode to a Lorentzian, we determine the cavity energy decay rate to be $\kappa/2\pi = 29.0 \pm 0.2$ GHz ($Q = 11\,900$) (all error bounds quoted in this paper are based on a 90% confidence bound for the nonlinear regression). The cavity-waveguide coupling rate is determined to be $\kappa_{||}/2\pi = 2.9 \pm 0.1$ GHz by measuring

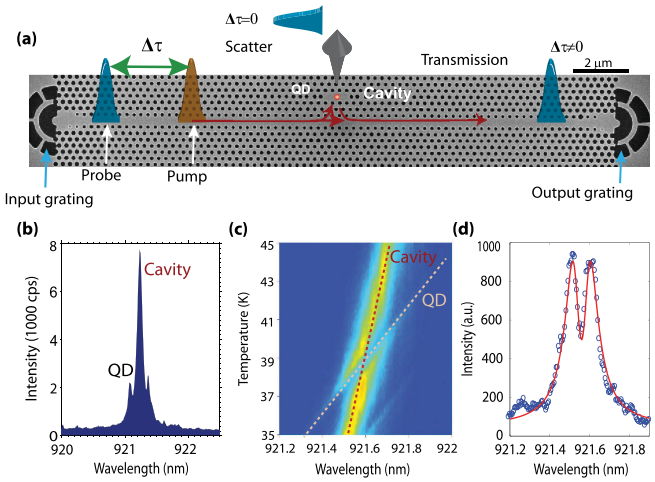

FIG. 1 (color online). (a) Scanning electron micrograph showing a fabricated device and illustrating pump-probe measurement. A pump and probe field with relative time delay $\Delta\tau$ are injected into the waveguide via grating couplers. Probe transmission depends on whether the two pulses excite the cavity simultaneously or at different times. (b) Low power PL measurement of the cavity. (c) Cavity scatter under broadband LED excitation as a function of temperature. Dotted lines indicate the temperature dependence of QD and the cavity. (d) Scattering spectrum taken at 39 K when the QD is resonant with the cavity.

the waveguide transmission at a temperature of 51 K when the QD is well detuned from the cavity mode [11]. The fraction of power coupled to the cavity from the waveguide is given by $1-(1-r_0)^2=0.36$ where $r_0=2\kappa_{||}/\kappa=0.2$. Thus, the in-plane coupling rate reported here offers a good trade-off between high cavity Q for strong coupling and efficient cavity excitation through the waveguide. The coupling efficiency of the grating couplers is also measured by observing the Stark shift on the detuned QD as a function of incident pump power, as described in Ref. [16]. From these measurements we determine the coupling efficiency into the waveguide from the out-of-plane direction to be $\eta=0.008$. Full details of the measurement of the cavity-waveguide coupling rate and input coupling efficiency for the device used in this work are provided in the Supplemental Material [18].

Figure 1(c) shows the resonant cavity scattering spectrum as a function of temperature when the waveguide is excited by a broadband LED that serves as a white light source. Light is collected directly from the cavity mode and is measured via a grating spectrometer with a resolution of 23 μeV. As the temperature is increased, the QD identified in Fig. 1(b) redshifts and becomes resonant with the cavity. The scattering spectrum exhibits an anticrossing as the QD is tuned across the cavity mode due to strong coupling [7–10]. Figure 1(d) shows the measured scattering spectrum taken at 39 K when the QD is resonant with the cavity, which exhibits a doublet representing the two polariton modes. The solid line in Fig. 1(d) is a theoretical fit assuming a Jaynes-Cummings interaction model [11,19]. From the theoretical fit, we determine the cavity-QD coupling strength to be $g/2\pi=13.4\pm0.2$ GHz, and the QD linewidth to be $\gamma_{qd}/2\pi=5.8\pm0.5$ GHz. The fact that $g>\kappa/4$ ensures that the system is operating in the strong coupling regime.

The nonlinearity of the device is first studied under continuous wave excitation by injecting a second pump field from a narrowband tunable external cavity diode into the input grating along with the broadband LED. The pump field is detuned from the cavity resonance by 35 GHz. Figure 2 plots the resulting scattering spectrum, taken when the QD is resonant with the cavity, for both 0.1 μW [panel (a)] and 14.5 μW [panel (b)] pump power, measured after the focusing lens. The dashed red line shows the scattering spectrum when only the pump is present. At 14.5 μW of pump power, indirect emission from the cavity polaritons is observed due to the inelastic scattering of the pump laser, an effect that has been previously reported in a number of works [20–23]. The blue curve shows the elastic scattering spectrum of the broadband LED when injected with the pump, where we have subtracted the inelastic scattering contribution. At 0.1 μW, the pump field is weak and does not affect the cavity scatter, which exhibits a dip at the bare QD resonant frequency. As the pump power is increased to 14.5 μW, the position of the dip induced by the QD is redshifted due to the optical Stark effect [16,24–26]. In addition, the contrast of the dip is partially reduced due to the saturation of the QD by the strong pump field. These effects combine to enable the pump field to optically modify the cavity scatter and waveguide transmission, providing the possibility for all-optical switching. We note that the contrast of the dip in Fig. 2 is reduced as compared to Fig. 1(d). This reduction in contrast occurs because the sample is excited with a large LED power in order to minimize the relative contribution of inelastic photons from the pump. The large LED power partially saturates the QD resulting in a degraded contrast. In addition, it is also noted that in panel (b) the dip in the inelastic scattering contribution does not line

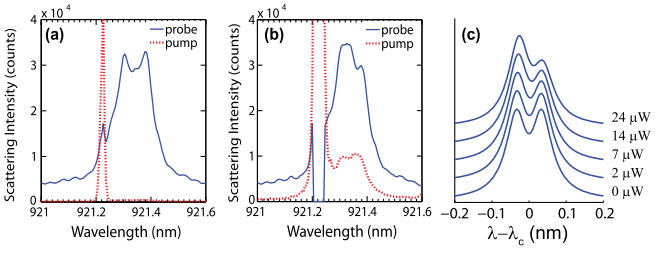

FIG. 2 (color online). Cavity scattering spectrum for (a) 0.1 μW and (b) 14.5 μW pump field powers. The dashed red line shows the cavity scattering spectrum with only the pump field (no signal). The solid blue line shows the scattering spectrum of the probe, with the pump scatter subtracted. (c) Theoretical scattering spectrum as a function of incident pump power before the grating.

up with the dip of the elastic scattering spectrum. This behavior is fully expected and is consistent with the predicted behavior of a two-level system strongly coupled to a cavity. Additional discussion on this point is included in the Supplemental Material [18].

The measured elastic scattering spectra can be compared to theoretical predictions based on numerical solution of the master equation [27]. The details for these calculations are provided in the Supplemental Material [18]. All calculations are performed using an open source quantum optics toolbox [28]. The calculated spectra are plotted in Fig. 2(c) for several different values of the pump power, defined as the power incident on the grating coupler. At low powers, the spectrum exhibits a doublet feature consistent with the measured spectrum shown in Fig. 2(a). As the pump power is increased, the elastic scattering spectrum becomes asymmetric due to the Stark shift of the QD, which is consistent the measured spectrum in Fig. 2(b). In addition, the contrast of the dip is reduced due to QD saturation. At even higher powers, the linewidth of the lower polariton experiences power induced broadening [16,23], leading to a broader line shape.

In order to dynamically modify the cavity spectrum on fast time scales, the sample is excited with a pump and probe laser pulse generated from two synchronized Ti: sapphire lasers. The pump laser has a pulse duration of 140 ps. The probe laser, whose initial pulse duration is 5 ps, is filtered down to a bandwidth of 0.02 nm (7 GHz) using a Fabry-Perot cavity, resulting in a 45 ps exponential pulse. The bandwidth of the probe laser is chosen to be approximately one quarter of the spectral width of the dip induced by the QD in the cavity scattering spectrum, which is equal to $2g$ in the strong coupling regime. The pump pulse is synchronized to the probe by a piezo feedback in the laser cavity, and the delay between the two pulses is controlled electronically by a phase-locked loop in the synchronization circuit. The wavelength of the pump and probe fields are selected such that when the QD is resonant with the cavity mode, the probe is resonant with the bare QD frequency while the pump wavelength is resonant with the lower polariton. The average pump power is set to 1 μW, while the probe power is set to 40 nW to ensure that it is in the linear response regime of the cavity-QD system. Temperature tuning is used to tune the QD through the probe field center frequency. The pump and probe fields are collected either directly from the cavity or from the output coupler, and are separated by a grating spectrometer.

Figure 3(a) shows the probe scattering intensity collected directly from the cavity as a function of temperature when the delay between pump and probe is set to either 0 ns (simultaneous excitation) or 4 ns. The 4 ns delay is chosen because it is much larger than all the decay times of the cavity-QD system. In this case, the pulses excite the cavity at different times and therefore do not interact. The

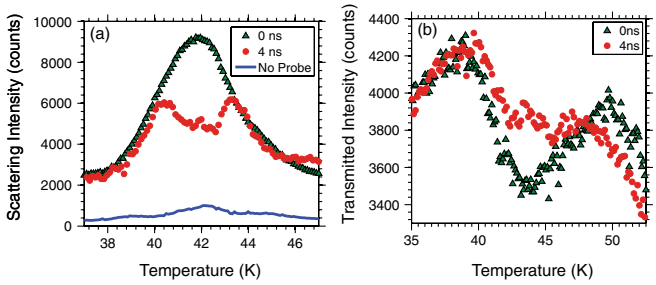

FIG. 3 (color online). Probe scattering intensity as a function of sample temperature for delays of 0 (green triangles) and 4 ns (red circles), (a) collected from the cavity and (b) collected from the output coupler. Scattering spectrum with the pump only indicated as a solid blue line in panel (a).

probe scattering is suppressed when resonant with the QD (42 K) due to cavity-QD interactions. We note that the temperature where resonance is achieved is slightly different than that of Fig. 1(c) because of a gradual redshift of the cavity resonance frequency observed over the course of the measurement process. When the pump and probe arrive simultaneously at the cavity (0 ns delay), a significant increase of the cavity scatter is observed at the same temperature. The switching contrast in the scattering spectrum, defined as $\eta_s = (I^S_{\max} - I^S_{\min})/I^S_{\max}$ where $I^S_{\max}$ and $I^S_{\min}$ are the probe scattering intensities at 0 and 4 ns delays, respectively, taken at 42 K sample temperature, is calculated to be 0.44.

In Fig. 3(a) the scattering spectrum is also plotted for the case where only a control pulse is injected (solid blue line). In this case, there is still some optical energy at the QD frequency, which is mostly dominated by the spectral overlap between the signal and control. In contrast to the continuous wave measurements shown in Fig. 2(b), inelastic scattering of pump photons contributes very little in the pulsed measurements. We attribute this difference to the fact that the measured inelastic scattering intensity is proportional to the average control power while the Stark shift and saturation are proportional to peak control power. In the pulsed operation, we can achieve a high peak power with a relatively low average power, which significantly reduces the inelastic scattering contribution.

In addition to the cavity scattering intensity, the waveguide transmission intensity can also be measured by collecting the probe field from the output coupler. The results of this measurement are shown in Fig. 3(b). At the output coupler, the spectrum exhibits the conjugate effect. At the 0 ns delay the transmission exhibits an antiresonance, while at 4 ns a double antiresonance can be observed. This double antiresonance is consistent with the continuous wave measurement of the waveguide transmission spectrum, as described in the Supplemental Material [18]. The switching contrast in transmission is calculated to be $\eta_t = (I^T_{\max} - I^T_{\min})/I^T_{\max} = 0.13$, where $I^T_{\max}$ and $I^T_{\min}$ are the probe transmitted intensities at 0

and 4 ns delays, respectively, taken at 43 K sample temperature, which is significantly lower than η_s. This reduction results from the fact that η_t is limited by the bare cavity transmission contrast denoted $\Delta T = 1 - (1 - r_0)^2$, where $r_0 = 2\kappa_{||}/\kappa$. Using the values of $\kappa_{||}/2\pi = 2.9$ GHz and $\kappa/2\pi = 29$ GHz measured under continuous wave excitation, we determine that $\Delta T = 0.36$. In the Supplemental Material, it is shown that $\eta_t \leq \Delta T$ with equality attained in the limit $C = 2g^2/\gamma_{qd}\kappa \gg 1$, where C is the atomic cooperativity [18]. A relationship between η_t, η_s, and ΔT is also derived and used to calculate ΔT, which is shown to be consistent with the value measured under continuous wave excitation when the bandwidth of the probe pulse is properly taken into account.

To measure the switching time of the system, the sample temperature is fixed at the strong coupling point and the cavity scatter is measured as a function of the delay between pump and probe. The measurement results are shown in Fig. 4. The scatter exhibits a sharp peak near the 0 ns delay. The temporal response of the system is asymmetric due to the fact that the probe pulse is filtered by a Fabry-Perot cavity and is therefore an asymmetric exponential pulse. The pump pulse shape was also measured using a high speed detector and found to be asymmetric. We fit the scattering intensity to a double-sided exponential of the form $S(\tau) = A[\exp(\tau/t_r)\Phi(-\tau) + \exp(-\tau/t_f)\Phi(\tau)]$ where $\Phi(\tau)$ is a unit step function, A is a normalization constant, and t_r (t_f) is the rise (fall) time of the response. The optimal fit is attained for $t_r = 47 \pm 10$ ps and $t_f = 127 \pm 19$ ps. The switching time, defined by the full width half maximum width, is $\Delta\tau = 120 \pm 15$ ps. This switching time is limited by the pulse duration of the pump and probe. Using a faster pump pulse would reduce this time, but may also necessitate using a shorter probe pulse duration that would decrease the switching contrast due to the finite acceptance bandwidth of the transmission dip shown in Fig. 1(d). In the strong coupling regime, the bandwidth of the transmission dip is approximately equal to $2g$. The probe pulse duration must be longer than $g^{-1} = 12$ ps (assuming a transform limited Gaussian pulse shape) to fit within this bandwidth, which sets the fundamental limit for the switching response time.

Figure 5(a) plots the relative change in probe scattering intensity, defined as $\beta = (I^S_{\max} - I)/(I^S_{\max} - I^S_{\min})$ where I is the scattering intensity and $I^S_{\max}$ and $I^S_{\min}$ are previously defined, as a function of the pump strength. The bottom axis indicates the pump strength in units of photons per pulse propagating in the waveguide mode, calculated using $E = P_{\text{inc}}\eta/\hbar\omega_p R$ where $R = 76.3$ MHz is the laser repetition rate, $\eta = 0.008$ is the grating coupler efficiency, and ω_p is the frequency of the pump pulse. The top axis indicates the pump strength in units of average pump power incident on the grating coupler, denoted P_{inc}. Measurements in Fig. 5(a) are shown for three different values of $\Delta = \omega_p - \omega_{qd}$, where the probe is always set to be resonant with the bare QD frequency ω_{qd}. For each curve, as the pump pulse energy is increased, the device makes a smooth transition from $\beta = 1$ to an asymptotic value of $\beta = 0$ at high pump energies. The pulse energy required to achieve switching increases with increased detuning, which is expected because fewer pump photons couple to the cavity mode.

The lines in Fig. 5(a) plot the theoretically predicted switching curve obtained by numerical integration of the master equation. A single fitting parameter is introduced into the simulation to relate the simulated driving amplitude of the cavity to the pump pulse energy. This fitting parameter accounts for variations in the pump pulse duration, which was found to change substantially depending on the laser cavity alignment, as well as the potential imperfect alignment of the pump field to the grating coupler. A detailed description of these numerical calculations is provided in the Supplemental Material [18]. The calculated solutions exhibit very good agreement with the experimental measurements. In addition to the switching curves, two horizontal lines are plotted which represent the 3 and 10 dB change in β. We define the pulse energy

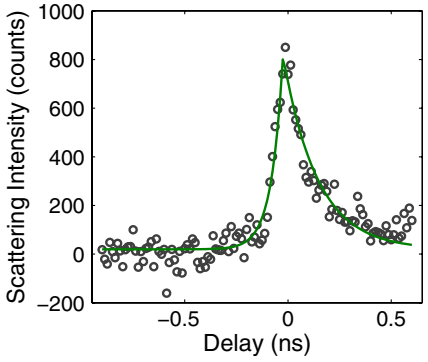

FIG. 4 (color online). Cavity probe scattering intensity as a function of pump-probe delay. The solid line represents theoretical fit.

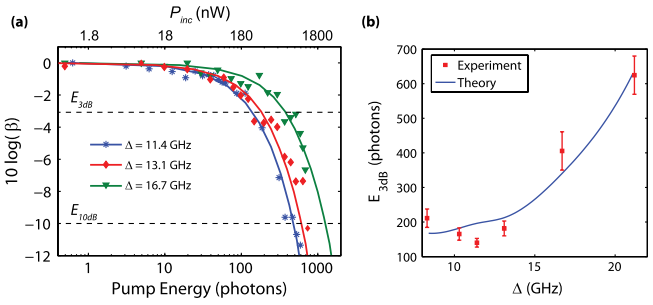

FIG. 5 (color online). (a) Switching contrast as a function of the pump pulse energy (in the waveguide) for three different values of $\Delta = \omega_p - \omega_{qd}$. Solid lines indicate the numerically calculated values. (b) Plot of $E_{3\,\text{dB}}$ as a function of Δ. The solid line represents numerically calculated values.

where these lines and the theoretical switching curves intersect as the 3 and 10 dB switching energies of the device, denoted $E_{3\,\mathrm{dB}}$ and $E_{10\,\mathrm{dB}}$, respectively. For $\Delta = 11.4$ GHz, we attain $E_{3\,\mathrm{dB}} = 140$ and $E_{10\,\mathrm{dB}} = 440$ photons, respectively. Figure 5(b) plots the measured value $E_{3\,\mathrm{db}}$ as a function of Δ, along with the numerically calculated values from the master equation. Numerical calculations are performed using a single fitting parameter to relate the simulated driving amplitude to the pump pulse energy for all detunings. Both experiment and theory indicate that when $\Delta < g$ the nonlinearity is not a strong function of the pump detuning. This behavior is explained by the fact that in this regime, Δ is less than the modified spontaneous emission rate of the QD, which ultimately limits the nonlinearity of the system.

In conclusion, we have demonstrated fast optical switching at ultralow energies by utilizing strong coupling between a QD and photonic crystal cavity. In our current device, only 36% of the pump energy from the waveguide couples to the cavity mode. By using better device designs this coupling efficiency could be significantly improved [29] to further reduce the switching energy. Ultimately, the minimum energy required to perform switching is given by the steady state energy stored in the cavity which is estimated from coupled-mode theory [30] to be $E_{\mathrm{cav}} = 2r_0/(\kappa\tau_c)E_{\mathrm{switch}} = 2$ photons. This limit could be achieved by pulse shaping of the pump field to match the cavity lifetime in order to enable nonlinearties near the single photon level, which are of great importance in quantum optics and quantum information.

D. Sridharan and R. Bose contributed equally to this work. The authors would like to acknowledge support from a DARPA Defense Science Office grant (Grant No. W31P4Q0910013), the Physics Frontier Center at the Joint Quantum Institute, the Office of Naval Research Applied Electromagnetics Center, the Army Research Office MURI on hybrid quantum interactions (Grant No. W911NF09104), and a National Science Foundation CAREER grant (Grant No. ECCS-0846494).

Note added in proof.—We would like to acknowledge related work by Englund *et al.* [31] that recently appeared.

*edowaks@umd.edu

[1] D. A. B. Miller, Nature Photon. **4**, 3 (2010).
[2] I. L. Chuang and Y. Yamamoto, Phys. Rev. A **52**, 3489 (1995).
[3] K. Nemoto and W. J. Munro, Phys. Rev. Lett. **93**, 250502 (2004).
[4] P. van Loock, T. D. Ladd, K. Sanaka, F. Yamaguchi, K. Nemoto, W. J. Munro, and Y. Yamamoto, Phys. Rev. Lett. **96**, 240501 (2006).
[5] K. Hinton, G. Raskutti, P. M. Farrell, and R. S. Tucker, IEEE J. Sel. Top. Quantum Electron. **14**, 938 (2008).
[6] T. Yoshie, A. Scherer, J. Hendrickson, G. Khitrova, H. M. Gibbs, G. Rupper, C. Ell, O. B. Shchekin, and D. G. Deppe, Nature (London) **432**, 200 (2004).
[7] S. Hughes and H. Kamada, Phys. Rev. B **70**, 195313 (2004).
[8] E. Waks and J. Vuckovic, Phys. Rev. Lett. **96**, 153601 (2006).
[9] D. Englund, A. Faraon, I. Fushman, N. Stoltz, P. Petroff, and J. Vuckovic, Nature (London) **450**, 857 (2007).
[10] J.-T. Shen and S. Fan, Phys. Rev. A **79**, 023837 (2009).
[11] R. Bose, D. Sridharan, G. S. Solomon, and E. Waks, Opt. Express **19**, 5398 (2011).
[12] E. Waks and J. Vuckovic, Phys. Rev. A **73**, 041803 (2006).
[13] A. Auffeves-Garnier, C. Simon, J. M. Gerard, and J. P. Poizat, Phys. Rev. A **75**, 053823 (2007).
[14] K. Srinivasan and O. Painter, Nature (London) **450**, 862 (2007).
[15] I. Fushman, D. Englund, A. Faraon, N. Stoltz, P. Petroff, and J. Vuckovic, Science **320**, 769 (2008).
[16] R. Bose, D. Sridharan, G. S. Solomon, and E. Waks, Appl. Phys. Lett. **98**, 121109 (2011).
[17] A. Faraon, I. Fushman, D. Englund, N. Stoltz, P. Petroff, and J. Vuckovic, Opt. Express **16**, 12154 (2008).
[18] See Supplemental Material at http://link.aps.org/supplemental/10.1103/PhysRevLett.108.227402 for details of device characterization and numerical simulations.
[19] E. Waks and D. Sridharan, Phys. Rev. A **82**, 043845 (2010).
[20] M. Winger, T. Volz, G. Tarel, S. Portolan, A. Badolato, K. J. Hennessy, E. L. Hu, A. Beveratos, J. Finley, V. Savona *et al.*, Phys. Rev. Lett. **103**, 207403 (2009).
[21] S. Ates, S. M. Ulrich, A. Ulhaq, S. Reitzenstein, A. Loffler, S. Hofling, A. Forchel, and P. Michler, Nature Photon. **3**, 724 (2009).
[22] D. Englund, A. Majumdar, A. Faraon, M. Toishi, N. Stoltz, P. Petroff, and J. Vuckovic, Phys. Rev. Lett. **104**, 073904 (2010).
[23] A. Majumdar, A. Faraon, E. D. Kim, D. Englund, H. Kim, P. Petroff, and J. Vučković, Phys. Rev. B **82**, 045306 (2010).
[24] X. Xu, B. Sun, P. R. Berman, D. G. Steel, A. S. Bracker, D. Gammon, and L. J. Sham, Science **317**, 929 (2007).
[25] G. Jundt, L. Robledo, A. Högele, S. Fält, and A. Imamoğlu , Phys. Rev. Lett. **100**, 177401 (2008).
[26] A. Muller, W. Fang, J. Lawall, and G. S. Solomon, Phys. Rev. Lett. **101**, 027401 (2008).
[27] D. Walls and J. Milburn, *Quantum Optics* (Springer, New York, 2010).
[28] M. T. Sze, J. Opt. B **1**, 424 (1999).
[29] Y. Huo, S. Sandhu, J. Pan, N. Stuhrmann, M. L. Povinelli, J. M. Kahn, J. S. Harris, M. M. Fejer, and S. Fan, Opt. Lett. **36**, 1482 (2011).
[30] K. Nozaki, T. Tanabe, A. Shinya, S. Matsuo, T. Sato, H. Taniyama, and M. Notomi, Nature Photon. **4**, 477 (2010).
[31] Englund *et al.*, Phys. Rev. Lett. **108**, 093604 (2012).